Journal of Materials Chemistry A

Accepted Manuscript

ROYAL SOCIETY OF CHEMISTRY

www.rsc.org/materialsA

Journal Name

ARTICLE

Titanium oxynitride microspheres with the rock-salt structure for visible-light photocatalysts

Received 00th January 20xx,
Accepted 00th January 20xx

DOI: 10.1039/x0xx00000x

www.rsc.org/

Jung Bo Yoo[a], Hyo Jin Yoo[a], Hyuk Joon Jung[a], Han Sol Kim[a], Sora Bang[a], Jongmyung Choi[a], Hoyoung Suh[b], Ji-Hyun Lee[b], Jin-Gyu Kim[b], and Nam Hwi Hur[a,*]

Novel photocatalysts (TiO_2@$TiO_{1-x}N_x$) with the core-shell geometry were synthesized by controlled nitridation of the TiO_2 microspheres using ammonia gas. The oxynitride phases ($TiO_{1-x}N_x$) with cubic rock-salt structure are exclusively formed on the surface of the TiO_2 microspheres while the core of the microsphere retains TiO_2 phase without nitrogen doping. Various spectroscopic data confirm the formation of the core-shell structure, denoted as TiO_2@$TiO_{1-x}N_x$. The TiO_2@$TiO_{1-x}N_x$ materials showed superior photocatalytic activities for the decomposition of methylene blue as well as the generation of photocurrent under visible-light. It is evident that the $TiO_{1-x}N_x$ phase is the key element to induce the photocatalytic activity. Specifically, the partial doping of nitrogen into the TiO matrix is crucial for the visible-light absorption.

Introduction

Titanium dioxide (TiO_2) has been extensively studied because of its wide applications in solar-driven environmental and energy technologies since Honda and Fujishima discovered water splitting on a TiO_2 electrode under UV light.[1] TiO_2 has several merits as a photocatalyst including large abundance, low toxicity, and excellent stability.[2,3] However, a major drawback is that it absorbs only UV light due to its large band gap energy (3.0 and 3.2 eV for the rutile and anatase phases, respectively).[4,5] A wide range of approaches have been explored to narrow the band gap of TiO_2. Chen et al. reported that disordered TiO_2 nanoparticles (NPs) prepared by hydrogenation method exhibit significantly enhanced activity in the production of hydrogen (H_2) from water under visible-light.[6] The chemical composition of TiO_2 was also modified by doping nonmetal atoms such as carbon (C), hydrogen (H), nitrogen (N), fluorine (F), and sulfur (S) into the oxygen (O) site.[7-13] The dopants typically generate impurity states above the valence band of TiO_2, which results in the upshift of the valence band edge and the improvement in the solar absorption efficiencies of TiO_2. In particular, N-doped TiO_2 (nominally $TiO_{2-x}N_x$) materials with low N content (~ 1 wt %) have been thoroughly studied.[10,14] They are typically prepared by annealing TiO_2 at temperatures below 600 °C under ammonia (NH_3) atmosphere, which exhibit the excellent catalytic activities in the visible light range. But their absorption is not fully covered in the solar spectrum. Moreover, $TiO_{2-x}N_x$ is unstable after going through photocatalytic reaction and easily returns to parent TiO_2.

Despite the extensive interest in the N-doping in the TiO_2 matrix, there are few studies on the N-doped titanium monoxide (TiO) materials with cubic rock-salt structure due to the difficulty to control the doping level and the metallic character of TiO.[15,16] Simon et al. reported the synthesis of N-doped TiO NPs using laser pyrolysis, which shows a large shift of the absorption threshold in the visible region.[17] Similar to TiO, titanium nitride (TiN) also adopts cubic rock-salt structure and is considered to be metallic. In contrast to bulk TiN materials, TiN film prepared by a cathodic arc technique has a band gap of about 2.0 eV, indicating that TiN can be semiconducting if the particle size reduces to the nanometer scale.[18] Very recently, Zheng et al. prepared the TiO_xN_y@TiN composites through the flash oxidation of commercial TiN particles, demonstrating a high photocatalytic activity for H_2 production under visible light irradiation.[19] However, the non-equilibrium quick oxidation of TiN particles in the presence of 2,4,6-trinitrophenol hampers controlling of optimal doping level.

[a] Department of Chemistry, Sogang University, Seoul 121-742, Korea
[b] Nano-Bio Electron Microscopy Research Group, Korea Basic Science Institute, Daejeon 34133, Korea

† Footnotes relating to the title and/or authors should appear here.
Electronic Supplementary Information (ESI) available: [details of any supplementary information available should be included here]. See DOI: 10.1039/x0xx00000x

Here we report a convenient and reproducible method to make a new visible-light active composite photocatalyst. Controlled nitridation of monodisperse TiO_2 microspheres, accomplished by flowing ammonia gas, converted the shell into the $TiO_{1-x}N_x$ phase and transformed the core into the amorphous TiO_2 phase. As a result, the nitrided product has the core-shell type structure, which is composed of two phases: a crystalline $TiO_{1-x}N_x$ phase as a shell and an amorphous TiO_2 phase as a core. Hereafter, we denote it as $TiO_2@TiO_{1-x}N_x$. The $TiO_2@TiO_{1-x}N_x$ material exhibited excellent photocatalytic activities under visible-light, including the degradation of methylene blue and the production of photocurrent. The nitrogen doping in $TiO_{1-x}N_x$ is considered to be responsible for absorbing visible light.

Experimental section

Chemicals All chemicals were purchased from commercial suppliers and were used without further purification unless otherwise stated. Ethanol, dodecyl amine (98%, DDA), methylene blue (MB), terephtalic acid (98%), sulfuric acid (>95%), and Nafion were purchased from Sigma-Aldrich (St Louis, USA). titanium tetraisopropoxide (TTIP) were obtained from Tokyo Chemical Industry (Tokyo, Japan).

Synthesis of monodisperse TiO_2 microspheres Monodisperse TiO_2 microspheres were prepared using TTIP as the titanium source. In brief, 3 mL of DDA, 4 mL of deionized water, and 300 mL of ethanol were added to a round-bottom flask, and the solution was cooled to -20 ^{o}C and stirred for 1 h. Using a syringe, a solution containing 6 mL of TTIP and 8 mL of ethanol was injected into the cold solution. After vigorous stirring for 20 h at -20 ^{o}C, white precipitates that formed gradually were separated from the solution by centrifugation. The precipitates were sintered in air at 500 ^{o}C for 6 h, yielding 1.44 g of TiO_2 powders (89.2% yield based on TTIP). The powders are composed of evenly dispersed spherical microspheres and their average diameter is approximately 560 nm.

Synthesis of $TiO_2@TiO_{1-x}N_x$ microspheres The TiO_2 microspheres were annealed in NH_3 at 700 ^{o}C to yield the desired $TiO_2@TiO_{1-x}N_x$ microspheres. The flow of ammonia gas was controlled using a mass flow controller. The flow rate is fixed at 300 standard cubic centimeters per minute. Six different samples were prepared by controlling the annealing time. The annealing was performed at 700 ^{o}C for 1, 4, 7, 10, 24, and 48 h. The white microspheres gradually became blue when the sample was annealed under the ammonia atmosphere.

Characterization Powder X-ray diffraction (XRD) data were collected using a Rigaku DMAX 2500 diffractometer (Cu Kα; Rigaku, Japan) operating at 40 kV and 150 mA. High resolution transmission electron microscopy (TEM) was performed using a JEOL JEM-2100F microscope (JEOL, Japan). Specimens for the TEM examinations were prepared by dispersing finely ground powders of the samples in anhydrous ethanol and then allowing a drop of the suspension to evaporate on a 400 mesh carbon-coated grid. High resolution scanning electron microscope (SEM) analyses were carried out using a Hitachi S-5500 microscope (Hitachi, Tokyo, Japan). Samples for the SEM analyses were prepared by dropping diluted samples in anhydrous ethanol on a lacey support grid. Samples were also subjected to chemical micro analyses using an Oxford Instruments INCA TEM 300 system (Oxford Instruments, Abingdon, UK) for energy dispersive X-ray (EDX) analysis. UV-visible absorption spectra of methylene blue (MB) solutions were recorded using a Perkin Elmer Lambda 950 spectrometer. The UV-Visible absorption spectra of the powders were measured using an integrating sphere accessory by the diffuse reflectance method. Raman spectra were obtained at 25 ^{o}C using a LabRam HR Raman spectrometer (Horiba Jobin-Yvon) equipped with a liquid-nitrogen-cooled CCD multichannel detector. A 514 nm Ar-ion laser was used as the excitation source. Photo luminescence spectra were measured on a Hitachi F-7000 fluorescence spectrophotometer. Thermal gravimetric analysis was carried out using a TGA 2050 instrument (TA Instruments). The sample was placed on a platinum pan for each run. The data were collected in air from 25 ^{o}C to 700 ^{o}C at the rate of 5 ^{o}C/min. Adsorption and desorption measurements were carried out at 77 K using an ASAP 2420 instrument (Micromeritics, USA) with nitrogen as the adsorptive gas. The Brunauer-Emmett-Teller (BET) surface areas were calculated using P/P_0 = 0.05 - 0.3 from the adsorption curve using the BET equation. The pore-size distributions were obtained from the desorption curve using the density functional theory method. Prior to each sorption measurement, the sample was out-gassed at 300 ^{o}C for 24 h *in vacuo* to completely remove the impurities. To investigate the elemental compositions, X-ray photoelectron spectroscopy (XPS; Theta probe AR-XPS System, Thermo Fisher Scientific, UK) analysis

using a mono-chromated Al Kα X-ray source (hν = 1486.6 eV) was performed at the Korea Basic Science Institute (KBSI) in Busan. The nitrogen contents of the TiO_2@$TiO_{1-x}N_x$ samples were analyzed using inductively coupled plasma atomic emission spectroscopy (ICP-AES, JY Ultima2C) at KBSI in Seoul.

Results and discussion

Monodisperse titanium oxynitride (TiO_2@$TiO_{1-x}N_x$) microspheres were prepared via two main pathways: (1) sol-gel synthesis of TiO_2 microspheres and (2) nitridation of the TiO_2 microspheres in NH_3. Uniform TiO_2 microspheres were prepared with solution of TTIP, DDA, deionized water, and ethanol. The solution temperature was maintained at -20 ^oC during the sol-gel polymerization process to make TiO_2 microspheres with virtually identical diameters as well as to prevent agglomeration. After separating white precipitates from the solution, white precipitates were then heated at 500 °C for 6 h, yielding white crystalline TiO_2 microspheres with average diameter of 560 nm. The TiO_2 microspheres were then nitrided at 700 °C in a NH_3 atmosphere for different periods of time. The white TiO_2 microspheres turned blue to deep blue, depending on the annealing time. This color change implies the formation of the rock-salt $TiN_{1-x}O_x$ phase in the TiO_2 microsphere.

As illustrated in Fig. 1, the TEM and SEM images of representative TiO_2@$TiO_{1-x}N_x$ microspheres clearly reveal that the size of parent TiO_2 microsphere was noticeably shrunk but the spherical shape appeared to be remained. The results implicate that the annealing is effective mostly on the surface of the TiO_2 microspheres at 700 °C. Average diameter of TiO_2@$TiO_{1-x}N_x$ microspheres nitrided for 24 h was reduced to about 420 nm, which was estimated from the TEM images of TiO_2@$TiO_{1-x}N_x$ in Fig. 1. When the sample was nitrided at 900 ^oC, however, the spherical shape was almost collapsed when the sample was nitrided for 24h at 900 ^oC (Fig. S1), indicating that annealing at high temperature completely converts oxide phase into nitride phase.

We first investigated the structures of the TiO_2@$TiO_{1-x}N_x$ microspheres with powder X-ray diffraction (XRD). The XRD data, given in Fig. 2, show that anatase TiO_2 phase is gradually transformed into $TiN_{1-x}O_x$ with cubic rock-salt structure as the nitridation time increases. The sample nitrided at 700 °C for 4 h shows that two new XRD peaks about 37.2^o and 43.2^o, which can be assigned to (111) and (200) reflections in $TiO_{1-x}N_x$, appear along

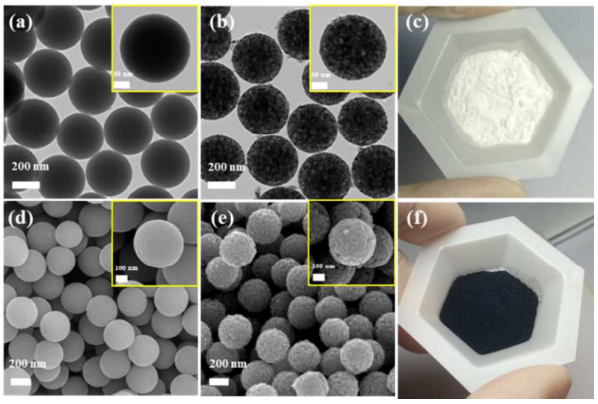

Fig. 1. TEM images of (a) parent TiO_2 and (b) nitrided TiO_2@$TiO_{1-x}N_x$ microspheres where nitridation was done at 700 °C for 24 h. Corresponding SEM images of (d) TiO_2 and (e) TiO_2@$TiO_{1-x}N_x$ microspheres. Photos comparing (c) white TiO_2 powders and (f) dark blue TiO_2@$TiO_{1-x}N_x$ samples are given in the right panel.

with the TiO_2 peaks.[20,21] This indicates that anatase TiO_2 phase coexisted with cubic $TiO_{1-x}N_x$ phase in short period of time. When the nitridation was prolonged to 10 h, the two peaks corresponding to cubic $TiO_{1-x}N_x$ became more distinctive in the XRD data while other peaks from anatase TiO_2 phase almost completely disappeared. This suggests that cubic $TiO_{1-x}N_x$ phase is predominantly formed on the surface of the TiO_2 microspheres nitrided for longer than 10 h. Average crystallite size of $TiO_{1-x}N_x$ synthesized by nitriding TiO_2 sample for 24 h, determined from half-peak widths in the XRD peak by applying the Scherrer equation, is 17.1 nm. Lattice parameters were calculated using the (111) and (200) reflections in the XRD data. Table S1 lists calculated lattice parameters for $TiO_{1-x}N_x$, along with the TiN and TiO standard data from the JCPDS file. Lattice constants of $TiO_{1-x}N_x$ nitrided for 24 h are approximately in the middle of those for TiN and TiO, indicating that both O and N atoms are randomly disordered in the anion sites of the rock salt structure.

It is worth mentioning that metallic TiN phase can be obtained only when the nitridation temperature was higher than 900 °C. This suggests that the nitridation at 700 °C results in partial replacement of oxygen in TiO_2 with nitrogen rather than complete substitution. In the course of nitridation, TiO_2 is the only oxygen source. It is thus conceivable that anion exchange between nitrogen and oxygen occurs initially at the surface of TiO_2. Hence, the TiO_2 microsphere annealed at 700 °C is composed of partially nitrided $TiO_{1-x}N_x$ and unreacted TiO_2 phases. Presumably the nitrided phase starts forming on the outer surface of a TiO_2 microsphere and gradually penetrates into the inner core via the oxygen exchange. As a result,

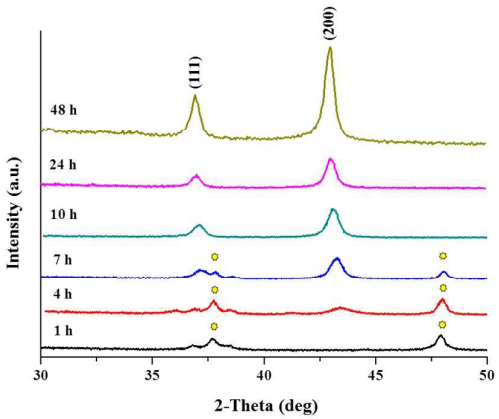

Fig. 2. Powder XRD patterns of TiO_2@$TiO_{1-x}N_x$ microspheres with different nitridation time. Two peaks were indexed on the basis of the JCPDS data. Peaks marked with an asterisk correspond to the TiO_2 peaks.

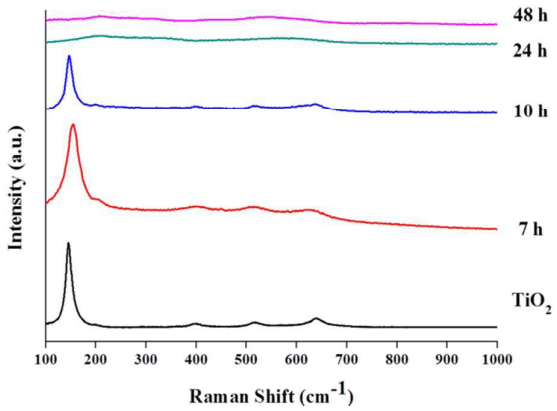

Fig. 3. Raman spectra of TiO_2@$TiO_{1-x}N_x$ microspheres with different nitridation time. For comparison, Raman spectrum of TiO_2 microspheres was displayed on the bottom.

the outer shell is predominantly composed of $TiO_{1-x}N_x$ whereas the inner core mainly consists of TiO_2, yielding the core/shell type microsphere. The XRD data suggest that the nitridation time and temperature strongly influences on the formation of $TiO_{1-x}N_x$ at the surface and the shell thickness. It is interesting to note that any XRD peaks corresponding to the TiO_2 phase were not displayed in the samples nitrided for 24 and 48 h although unreacted TiO_2 phase remains in the nitrided samples. The absence of the XRD peaks suggests that TiO_2 in the core part might exist as an amorphous state. Nitridation appears to induce the disordered state via the exchange between oxygen and nitrogen in the boundary, which results in the transformation of crystalline TiO_2 phase into amorphous TiO_2 state.[6,22] Another plausible cause is that X-ray might not penetrate enough into the inner core of the TiO_2 microsphere. The diffracted peaks are thus ascribed mainly to the $TiO_{1-x}N_x$ phase on the surface.

Raman spectroscopy was employed to confirm the structural changes by the nitridation time (Fig. 3). Anatase phase of TiO_2 has six Raman-active vibrational modes including one A_{1g} mode at 527 cm^{-1}, two B_{1g} modes at 382 and 504 cm^{-1}, and three E_g modes at 141, 154, and 654 cm^{-1}.[23] The samples nitrided at 700 °C for 7 h showed virtually identical Raman patterns owing to the anatase TiO_2 phase, suggesting that conversion of TiO_2 into $TiO_{1-x}N_x$ is not complete at this stage. However, the E_g mode at 154 cm^{-1} in the spectrum of the sample nitrided for 10 h was significantly blue-shifted and noticeably broadened relative to that in the TiO_2 spectrum, indicating that particle sizes were changed and defects were produced by nitridation. Raman spectrum of the TiO_2 microspheres nitrided for 24 h did not show any peaks corresponding to the anatase TiO_2 phase and exhibited very broad peaks at ~210, ~290, ~570 cm^{-1} due to the cubic $TiO_{1-x}N_x$ phase. The first-order Raman scattering is forbidden for the crystal with a cubic rock salt structure (space group: F_{m3m}) because every atom is located at a site of inversion symmetry.[24] Since $TiO_{1-x}N_x$ contains a wide range of vacancies and defects, however, the forbidden rule can be relaxed and Raman peaks can thus be observed.[25,26] The very broad peaks are probably associated with acoustic and optical modes of $TiO_{1-x}N_x$. It is worthy to mention that unreacted TiO_2 phase was not detected in the 24 h sample by Raman analysis. This indicates that structural

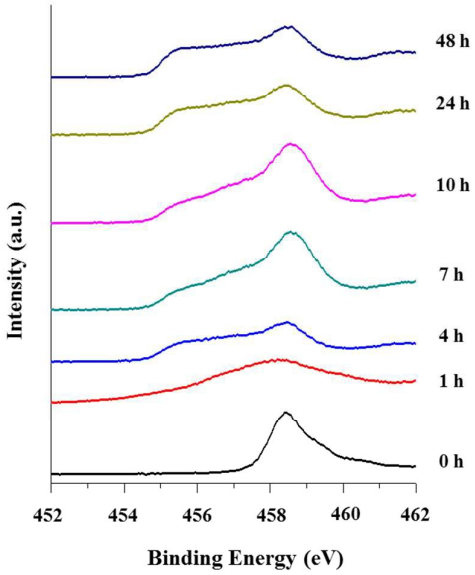

Fig. 4. Ti 2*p* XPS spectra of the TiO_2@$TiO_{1-x}N_x$ samples with different nitridation time.

changes occur after nitridation, resulting in oxygen disorders primarily in the TiO_2 phase in the core. The Raman data obtained from the nitrided samples are consistent with the XRD results.

The XRD and Raman results discussed above show the formation of cubic $TiO_{1-x}N_x$ phase but do not provide any direct evidence on the presence of unreacted TiO_2 phase. XPS data of the nitrided samples prepared by annealing at different dwell times were examined to assess the chemical environments and oxidation states of Ti and N. In particular, two important regions including Ti 2*p* and N 1*s* were carefully investigated for each sample. Fig. 4 shows the XPS spectra in the Ti 2*p* region (452-462 eV) of the TiO_2@$TiO_{1-x}N_x$ samples. The Ti 2*p* XPS spectra of the TiO_2 and nitrided samples exhibit drastic differences. The XPS data shows that the binding energy was shifted from higher to lower values with increased annealing time. The sharp peak at 458.3 eV is typical for the Ti $2p_{3/2}$ in anatase TiO_2, namely the Ti^{4+} species.[27,28] A notable feature is that the peak at 458.3 eV is observed regardless of the annealing time, suggesting that unreacted TiO_2 phase is present even if the sample was nitrided for over 24 h. The broader peaks in the range of 455 to 458 eV can be attributed to Ti^{2+}, Ti^{3+}, and Ti^{4+} species.[29,30]

For the sample nitrided for 24 h, the spectral curve was fitted with five peaks centered at 455.6, 457.2, 458.3, 461.4, and 464.0 eV, which is given in Fig. 5. The Ti $2p_{3/2}$ XPS peaks are typically observed in the range of 455 to 460 eV. The lowest peak at 455.6 eV is ascribed to the Ti^{2+} species that could be associated with TiO. A peak centered at 457.2 eV can be assigned to the Ti^{3+} of TiN or N-Ti-O bonding in $TiO_{1-x}N_x$.[31] The peak at 458.3 eV correlates to the Ti^{4+} in TiO_2. Two peaks at 461.4 and 464.0 eV are due to the Ti $2p_{1/2}$

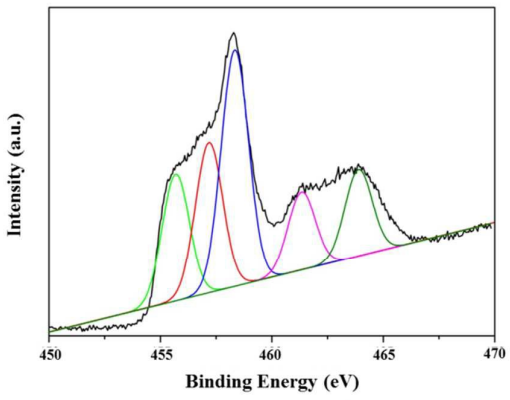

Fig. 5. Ti 2*p* XPS spectra of TiO_2@$TiO_{1-x}N_x$ which was prepared by nitriding for 24 h. The black line is an experimental XPS curve. The colored curves are the fittings of experimental XPS data, which can be decomposed into a superposition of five peaks shown as colored curves.

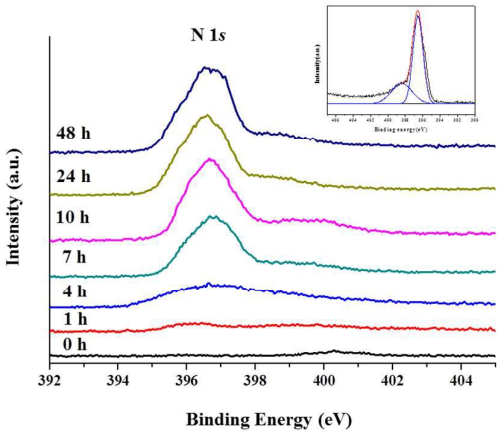

Fig. 6. N 1*s* XPS spectra of the TiO_2@$TiO_{1-x}N_x$ samples with different nitridation time. The inset is the fitting of experimental XPS data for the 24 h nitridation sample, which can be decomposed into a superposition of two peaks shown as blue curves. The black curve is XPS data.

spectra. One peak at 464.0 eV is ascribed to the Ti^{4+} of TiO_2 while the other at 461.4 eV is associated with the N-Ti-O bonding in the oxynitride phase such as $TiO_{1-x}N_x$. The Ti 2*p* XPS spectra suggest that the nitrided sample contains the multiple oxidation states of Ti and might be composed of TiO, $TiO_{1-x}N_x$, and TiO_2.

The presence of N in the nitrided sample was clearly evidenced by the N 1*s* XPS spectra of TiO_2@$TiO_{1-x}N_x$ shown in Fig. 6. The N 1*s* peaks are more distinctive with increasing nitridation time. For the sample nitrided for 7 h, a nearly single peak is observed. However, the samples with longer nitridation time showed a broad peak. The inset in Fig. 6 is the N 1*s* XPS spectrum of the 24 h sample. The red curve is the fitting data of experimental XPS data, which can be resolved into two peaks shown as blue curves. The first peak at 396.5 eV is characteristic of the N dopant which corresponds to the Ti-N bonding and the second one at 398.7 eV can be attributed to the N-Ti-O species.[32]

From the XRD, Raman, and XPS data, it is conceivable that the nitrided samples are composed of $TiO_{1-x}N_x$ and TiO_2. However, it is very difficult to determine how much TiO_2 phase in the parent TiO_2 microsphere remains intact during the nitridation procedure. Thus, TGA was employed to determine the nitrogen content, which is useful to estimate the approximate ratio of $TiO_{1-x}N_x$ to TiO_2 in TiO_2@$TiO_{1-x}N_x$. The TGA data of the nitrided samples were collected in air as a function of temperature. For comparative purpose, commercial TiN powder was also measured under the same conditions. All the samples were transformed into the rutile TiO_2 phase after measurements, which were confirmed by XRD.

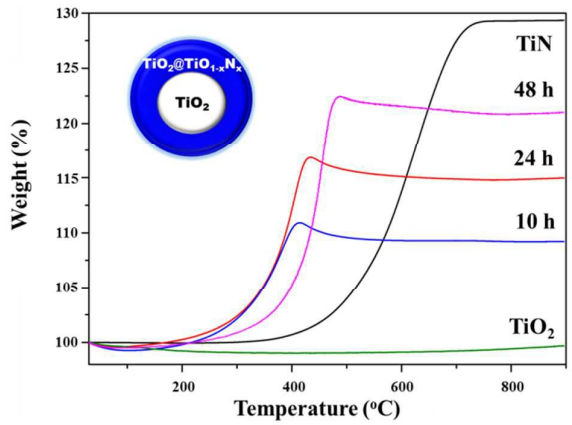

Fig. 7. Thermogravimetric analysis (TGA) data for the samples nitrided at 700 °C for 10 and 24 h. Data were collected in air at a heating rate of 10 °C per minute. For comparison, TGA data for TiN was included. The inset is a simplified drawing of a $TiO_2@TiO_{1-x}N_x$ microsphere with shell thickness of about 56 nm and core diameter of about 208 nm. The relative ratio of $TiO_{1-x}N_x$ to TiO_2 was determined on the basis of the TGA and EDX data for the sample nitrided at 700 °C for 24 h.

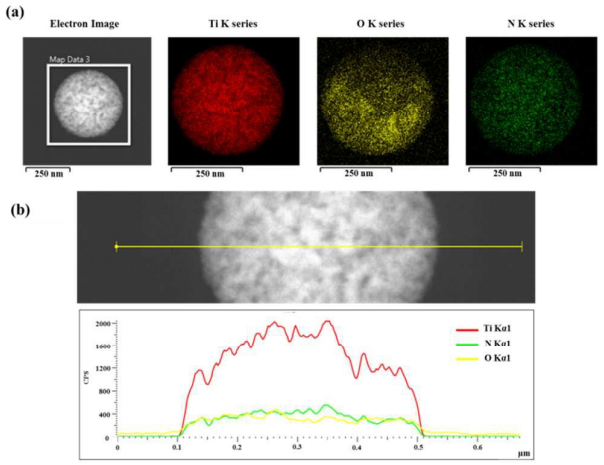

Fig. 8. (a) Elemental mapping images of $TiO_2@TiO_{1-x}N_x$ nitrided at 700 °C for 24 h by scanning TEM. (b) EDX line profiles of N, O, and Ti across the $TiO_2@TiO_{1-x}N_x$ interface.

As illustrated in Fig. 7, the weight percentage of TiN increases to about 129 %, which is close to the theoretical value for the conversion of TiN into TiO_2. In contrast, the weight gain of the sample nitrided at 700 °C for 24 h is about 115 %, which is much lower than that of TiN. This clearly suggests that unreacted TiO_2 phase remains in the nitrided samples. A notable feature is that the weight gains of the samples annealed for 24 and 48 h are not significantly different, supporting that the temperature annealed at 700 °C is not sufficient to completely convert TiO_2 into TiN.

Since the ratio of $TiO_{1-x}N_x$ to TiO_2 in the nitrided sample cannot be determined by the TGA data alone, the EDX elemental analysis was employed to help estimating the relative compositions in $TiO_2@TiO_{1-x}N_x$. Although the EDX data are not completely reliable due to several factors such as surface, elements, and the specimen features, the technique provides reasonably reliable elemental compositions particularly for insoluble inorganic materials like $TiO_2@TiO_{1-x}N_x$. Weight percentages of Ti and N of the samples nitrided for 10, 24, and 48 h were obtained directly from the EDX data and oxygen contents were calculated assuming that the samples are solely composed of Ti, N, and O. Table S2 gives weight percentages and atomic ratios for the three samples. As anticipated, the EDX data show that the nitrogen content increases as the annealing time increases.

Based on TGA and EDX data, the ratio of $TiO_{1-x}N_x$ to TiO_2 for the sample nitrided at 700 °C for 24 h is estimated to be 0.18. For this calculation, we assumed that $TiO_2@TiO_{1-x}N_x$ has a core-shell type structure because the nitridation occurs initially on the surface and gradually penetrates into the core. EDX data was taken to determine relative amount of N and O. As illustrated in the inset of Fig. 7, the shell thickness and the core diameter of $TiO_2@TiO_{1-x}N_x$ sample are 56 nm and 308 nm, respectively.

Fig. 8 shows elemental mapping images and EDX line scan elemental profiles of the sample nitrided at 700 °C for 24 h, clearly confirming the presence of N, O, and Ti. The Ti intensity is strong and the intensity profile along the line is a nearly dome-shape. On the other hand, the intensities of N and O are relatively weak and did not noticeably change along the line due to their low scattering power. The elemental mapping images indicate that N, O, and Ti are evenly dispersed on the spherical surface and also imply that $TiO_{1-x}N_x$ is mostly located on the outer portion of the shell.

As illustrated in Fig. 8, conventional TEM is very difficult to differentiate between core and shell components in $TiO_2@TiO_{1-x}N_x$ mainly because the L-shell peak of Ti (0.452 keV) and the K-shell peak of N (0.392 keV) were too close to distinguish their elemental intensities. We have thus investigated the structure and chemical composition of the bisected $TiO_2@TiO_{1-x}N_x$ microsphere with scanning transmission electron microscopy (STEM), electron energy loss spectroscopy (EELS), and energy-dispersive X-ray spectroscopy (EDS). A $TiO_2@TiO_{1-x}N_x$ microsphere nitrided at 700 °C for 10 h was used and approximately bisected by a focused ion beam (FIB). Fig. 9 presents the bisected STEM image and corresponding EDS elemental mapping images of Ti, O, and N. The Ti and O signals are evenly dispersed in the core and shell parts of the bisected sphere

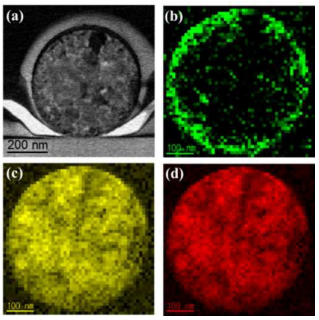

Fig. 9 (a) STEM images of a bisected TiO_2@$TiO_{1-x}N_x$ microsphere. Corresponding EELS mapping images of N (b, green), Ti (c, yellow), and O (d, red).

whereas the N signals are located exclusively on the shell of the sphere, indicating that the TiO_2@$TiO_{1-x}N_x$ microsphere has the core/shell structure. To further convince the compositions of the core and shell parts, we have investigated the STEM-EDS analysis of the bisected sample. As given in Fig. S2, the Ti, O, and N signals were observed in the shell part but only Ti and O signals were detected in the core. This clearly demonstrates that the $TiO_{1-x}N_x$ phase is formed on the shell by the nitridation but the core TiO_2 remains intact.

Diffuse reflectance UV-visible spectroscopy (DRUVS) was employed to determine whether the nitrided sample absorbs light effectively in the visible light region. The DRUVS spectrum of TiO_2@$TiO_{1-x}N_x$ nitrided at 700 ^{o}C for 24 h clearly shows that the sample absorbs much more light in the visible regions in comparison with that of TiO_2 (Fig. S3). Thus photocatalytic activity of TiO_2@$TiO_{1-x}N_x$ nitrided at 700 ^{o}C for 24 h was evaluated by measuring the degradation rate of methylene blue (MB) under visible light as a function of time. The absorbance of MB at 664 nm, which is the strongest peak of MB, was used to determine the concentration change of the MB solution.[33]

As shown in Fig. 10 (a), the strong absorption peak is continuously weakened with increasing irradiation time. This clearly indicates that the TiO_2@$TiO_{1-x}N_x$ catalyst efficiently decomposes MB under visible light. Similar efficient activities were also observed in all the samples nitrided at 700 ^{o}C. Among them, the sample nitrided for 24 h has the highest performance on the MB decomposition, which is given in Fig. 10 (b). Due to the large band gap energy (E_g = 3.2 eV) of TiO_2, the core TiO_2 is inactive in decomposition of MB under visible light. Therefore, it is evident that the $TiO_{1-x}N_x$ phase in the shell is the only active component in the visible range of irradiation and can be considered as a visible-light photocatalyst. This result is consistent with that of the DRUVS data.

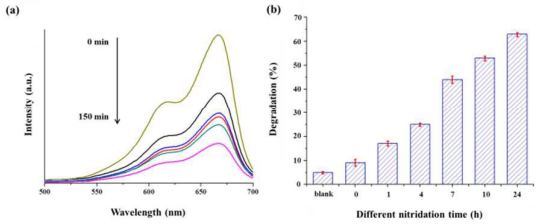

Fig. 10. (a) UV-visible spectra of the MB solution in the presence of TiO_2@$TiO_{1-x}N_x$ nitrided at 700 ^{o}C for 24 h under visible-light irradiation (> 420 nm) as a function of time of exposure to light. (b) Percentage of photocatalytic degradation of MB over the TiO_2@$TiO_{1-x}N_x$ samples with different nitridation time.

To elucidate whether hydroxyl radicals (•OH) produced from the illumination of TiO_2@$TiO_{1-x}N_x$ lead to the degradation of MB, we have employed the fluorescence technique that is usually used to estimate the formation of hydroxyl radicals on the surface of photocatalyst.[34-36] Fig. 11 showed the fluorescence spectral change of the terephthalic acid in the presence of TiO_2@$TiO_{1-x}N_x$ nitrided at 700 ^{o}C for 24 h with increasing irradiation time. A new peak about 425 nm, due to the hydroxylation product (2-hydroxyterephthalic acid), is distinctively displayed in the illuminated spectrum. The fluorescence intensity is gradually increased with increasing irradiation time. Based on these results, it is evident that the hydroxyl radicals generated from the TiO_2@$TiO_{1-x}N_x$ catalyst plays a significant role in the decomposition of MB.

In addition to the chemical degradation of MB by the hydroxyl radicals, we also evaluated the capability of photocurrent generation of the nitrided samples under visible light. The photocurrent density was clearly observed, which was very reproducible in the repeated on/off cycles of excitation.

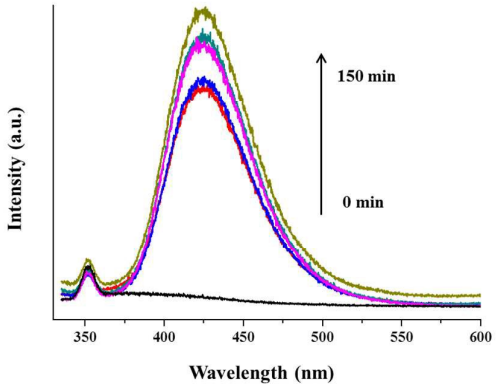

Fig. 11. Time-dependent fluorescence spectra obtained from the illumination of a NaOH solution of terephthalic acid in the presence of TiO_2@$TiO_{1-x}N_x$ nitrided at 700 ^{o}C for 24 h. Each spectrum was recorded every 30 min of illumination.

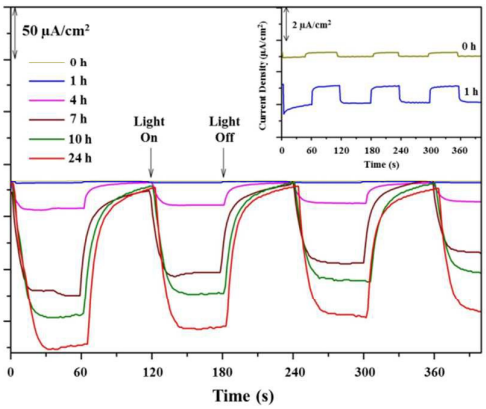

Fig. 12. Photocurrent response of the TiO_2@$TiO_{1-x}N_x$ samples with different nitridation time under an applied potential of 0.8 V (vs. Ag/AgCl) and a periodic irradiation of visible light.

As illustrated in Fig. 11, the photocurrent of the nitrided samples is enhanced when the nitridation time increased. The sample nitrided for 24 h has the largest value of photocurrent density (~170 μA/cm^2), which is comparable with that of carbon nitride (C_3N_4).[37,38] This clearly demonstrates that the TiO_2@$TiO_{1-x}N_x$ catalyst is able to generate photocurrents effectively under visible light while TiO_2 does not produce photocurrents under the same conditions.

Conclusions

The present study demonstrated the successful synthesis of new composite photocatalysts (TiO_2@$TiO_{1-x}N_x$) with enhanced visible light activity, which was accomplished by a controlled nitridation of TiO_2 microspheres. The nitrided products maintain a spherical shape and have unique core/shell structure. The core and shell parts are mainly composed of amorphous TiO_2 and crystalline $TiO_{1-x}N_x$ phases, respectively. They exhibited high photocatalytic and photoelectrochemical activities under visible light irradiation. Our structural and spectroscopic results confirm that the origin of their activity is due primarily to the $TiO_{1-x}N_x$ phase. Specifically, the nitrogen dopant in $TiO_{1-x}N_x$ appears to be responsible for photocatalytic activity under visible-light similar to well-documented N-doped TiO_2 phase ($TiO_{2-x}N_x$). Our studies on the $TiO_{1-x}N_x$ phase having a simple rock-salt structure promises a wide range of visible-light applications in both photocatalytic and photoelectrochemical systems.

Acknowledgements

We express gratitude to the editorial staff at Sogang University for the careful English revision of this manuscript.

Notes and references

1 A. Fujishima, K. Honda, *Nature,* 1972, **238**, 37-38.
2 X. B. Chen, S. S. Mao, *Chem. Rev.,* 2007, **107**, 2891-2959.
3 J. Huo, Y. Hu, H. Jiang, C. Li, *Nanoscale*, 2014, **6**, 9078-9084.
4 C. Dette, M. A. Pérez-Osorio, C. S. Kley, P. Punke, C. E. Patrick, P. Jacobson, F. Giustino, S. J. Jung, K. Kern, *Nano Lett.,* 2014, **14**, 6533-6538.
5 J. Zhang, P. Zhou, J. Liu, J. Yu, *Phys. Chem. Chem. Phys.*, 2014, **16**, 20382-20386.
6 X. Chen, L. Liu, P. Y. Yu, S. S. Mao, *Science*, 2011, **331**, 746-750.
7 J. C. Yu, J. Yu, W. Ho, Z. Jiang, L. Zhang, *Chem. Mater.,* 2002, **14**, 3808-3816.
8 S. Hoang, S. P. Berglund, N. T. Hahn, A. J. Bard, C. B. Mullins*, J. Am. Chem. Soc.,* 2012, **134**, 3659-3662.
9 J. Zhang, Y. Wu, M. Xing, S. A. K. Leghari, S. Sajjad, *Energy Environ. Sci.,* 2010, **3**, 715-726.
10 R. Asahi, T. Morikawa, T. Ohwaki, K. Aoki, Y. Taga, *Science*, 2001, **293**, 269-271.
11 M. Zhou, J. Yu, *J. Hazard. Mater.*, 2008, **152**, 1229-1236.
12 A. Naldoni, F. Fabbri, M. Altomare, M. Marelli, R. Psaro, E. Selli, G. Salviati, V. D. Santo, *Phys. Chem. Chem. Phys*., 2015, **17**, 4864-4869.
13 A. Naldoni, M. Allieta, S. Santangelo, M. Marelli, F. Fabbri, S. Cappelli, C. L. Bianchi, R. Psaro, V. D. Santo, *J. Am. Chem. Soc.*, 2012, **134**, 7600-7603.
14 J. Wang, D. N. Tafen, J. P. Lewis, Z. Hong, A. Manivannan, M. Zhi, M. Li, N. Wu, *J. Am. Chem. Soc.*, 2009, **131**, 12290-12297.
15 J. Graciani, S. Hamad, J. F. Sanz, *Phys. Rev. B*, 2009, **80**, 184112/1-184112/10.
16 S. G. Seo, C. Park, H. Kim, W. H. Nam, M. Jeong, Y. Choi, Y. S. Lim, W. Seo, S. Kim, J. Y. Lee, Y. S. Cho, *J. Mater. Chem. A*, 2013, **1**, 3639-3644.
17 P. Simon, B. Pignon, B. Miao, S. C-Leconte, Y. Leconte, S. Marguet, P. Jegou, B. B-Fabre, C. Reynaud, N. H-Boime, *Chem. Mater.*, 2010, **22**, 3704-3711.
18 V. Ern, A. C. Switendick, *Phys. Rev.*, 1965, **137**, A1927-A1936.
19 P. Zheng, J. Zhao, J. Zheng, G. Ma, Z. Zhu, *J. Mater. Chem.*, 2012, **22**, 12116-12120.
20 C. Gong, C. Yan, J. Zhang, X. Cheng, H. Pan, C. Zhang, L. Yu, Z. Zhang, *J. Mater. Chem.*, 2011, **21**, 15273-15278.
21 E. P. Quijorna, V. T. Costa, F. A-Rueda, P. H. Fernández, A. Climent, F. Rossi, M. M. Silván, *J. Phys. D: Appl. Phys.,* 2011, **44**, 235501/1-235501/8.
22 X. Chen, L. Liu, P. Y. Yu, S. S. Mao, *Science*, 2011, **331**, 746-750.
23 O. Frank, M. Zukalova, B. Laskova, J. Kürti, J. Koltai, L. Kavan, *Phys. Chem. Chem. Phys.*, 2012, **14**, 14567-14572.
24 A. T-Zajac, M. Radecka, K. Zakrzewska, A. Brudnik, E. Kusior, S. Bourgeois, M. C. Lucas, L. Imhoff, *J. Power Sources*, 2009, **194**, 93-103.
25 W. Spengler, R. Kaiser, H. Bilz, *Solid State Comm.*, 1975, **17**, 19-22.
26 W. Spengler, R. Kaiser, A. N. Christensen, G. M-Vogt, *Phys. Rev. B*, 1978, **17**, 1095-1101.
27 H. G. Yang, C. H. Sun, S. Z. Qiao, J. Zou, G. Liu, S. C. Smith, H. M. Cheng, G. Q. Lu, *Nature,* 2008, **453**, 638-642.
28 F. Peng, L. Cai, L. Huang, H. Yu, H. Wang*, J. Phys. Chem. Solids*, 2008, **69**, 1657-1664.

29 W. Göpel, G. Rocker, R. Feierabend, *Phys. Rev. B*, 1983, **28**, 3427-3438.
30 X. Song, D. Gopireddy, C. G. Takoudis, *Thin Solid Films*, 2008, **516**, 6330-6335.
31 M. Wolff, J. W. Schultze, H. H. Strehblow, *Surf. Interface Anal.*, 1991, **17**, 726-736.
32 I. Takahashi, D. J. Payne, R. G. Palgrave, R. G. Egdell, *Chem. Phys. Lett.*, 2008, **454**, 314-317.
33 W. Cai, G. Duan, Y. Li, Hierarchical Micro/Nanostructured Materials: Fabrication, Properties and Applications, CRC Press, Taylor and Francis Group, 2014.
34 J. Zhang, Y. Nosaka, *J. Phys. Chem. C*, 2013, **117**, 1383-1391.
35 L. Sun, Y. Qin, Q. Cao, B. Hu, Z. Huang, L. Ye, X. Tang, *Chem. Commun.,* 2011, **47**, 12628-12630.
36 T. P. Gujar, C. Anand, V. R. Shinde, J. Ye, K. Ariga, A. Vinu, *J. Nanosci. Nanotechnol.*, 2010, **10**, 8124-8129.
37 J. Fang, H. Fan, M. Li, C. Long, *J. Mater. Chem. A*, 2015, **3**, 13819-13826.
38 J. Liu, H. Wang, Z. P. Chen, H. Moehwald, S. Fiechter, R. Krol, L. Wen, L. Jiang, M. Antonietti, *Adv. Mater.*, 2015, **27**, 712-718.

Table of Contents (TOC) Graphic

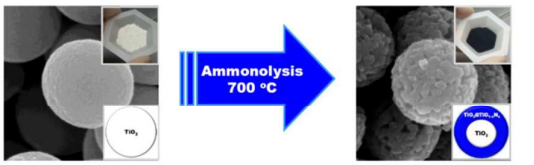

Novel photocatalysts (TiO_2@$TiO_{1-x}N_x$) with the core-shell structure, prepared by controlled nitridation of TiO_2 microspheres, show photocatalytic activity under visible-light irradiation